Parity nonconserving cold neutron-parahydrogen interactions

T. M. Partanen*

Department of Physical Sciences,P. O. Box 64,

FIN-00014 University of Helsinki, Finland

Abstract

Three pion dominated observables of the parity nonconserving interactions between the cold neutrons and parahydrogen are calculated. The transversely polarized neutron spin rotation, unpolarized neutron longitudinal polarization, and photon-asymmetry of the radiative polarized neutron capture are considered. For the numerical evaluation of the observables, the strong interactions are taken into account by the Reid93 potential and the parity nonconserving interactions by the DDH model along with the two-pion exchange.

* tero.partanen@helsinki.fi

I. INTRODUCTION

The knowledge of the strangeness conserving hadronic weak interaction relies completely on the parity nonconserving (PNC) observables. The PNC two-nucleon (NN) interactions provide a possible access to this least understood sector of the Standard Model. Experimentally such subtle particle spin control based PNC measurements are feasible but highly demanding. On the theoretical side, the challenge lies largely in the poorly known coupling values which parametrize the strength of the minuscule-sized PNC signal.

The PNC NN interaction is compelled to change either the spin or isospin of the system due to the Pauli exclusion principle and consequently the potential of the interaction is composed of various spin-isospin operators weighted by coupling constants. There are at least three considerable candidates for the PNC NN potentials. The new model-independent effective field theory (EFT) approach offers two alternative choices for these potentials, namely the pionless and pionful [1, 2]. The pionless one comprises only the short-range contact interaction whereas the pionful also the long- and medium-range interactions mediated respectively by the one- and two-pion exchanges. The third potential is the most conventional DDH meson-exchange model [3] which takes into account the long- and short-range effects in terms of the single $\pi^{\pm}, \rho$, and ω exchanges but not the two-pion exchange contributions which are supposedly important in the medium-range. In spite of the different approaches, the operators appearing in the potentials are essentially the same, except that the ranges of the force in them varies. Another similarity with the potentials is that they are all parametrized in terms of about half a dozen ill-known couplings. In EFT these so-called low energy constants are expected to be extracted from the experimental data of a series of prospective high-precision measurements. As a downside, the EFT potentials cannot be used in the evaluation of observables yet. Therfore, for over thirty years up until today, the theoretical predictions have largely rest on the DDH model and their recommended "best" values for the weak couplings. The PNC one-pion exchange potentials of the pionful EFT and DDH model coincide and are proportional to the weak $NN\pi$ coupling $h_\pi^{(1)}$. The strength of the PNC two-pion exchange is also dependent on the same coupling. Besides the DDH, there are various calculations [4–11] for the the $h_\pi^{(1)}$ (ranging between 0 and 3.4×10^{-7}) indicating a smaller value than what is the DDH "best" recommendation. The ongoing NPDGamma experiment [12] is hoped to reduce the vagueness related to the $h_\pi^{(1)}$ by mea-

suring with high accuracy the γ-asymmetry of the $\vec{n}p \to \gamma d$ at threshold known to be nearly a 100% pion exchange dominated.

Up till recently, the effect of the two-pion exchange has been considered small and neglected from the analyses of the PNC observables. However, recent calculations of the PNC longitudinal analyzing power $\bar{A}_L$ in the $\vec{p}p$ elastic scattering show the importance of the two-pion exchange [13, 14]. The PNC pp reaction offers an auspicious opportunity to study the two-pion exchange contribution for a couple of reasons. Firstly, the single pion-exchange does not appear according to Barton's theorem [15], from which it follows that the two-pion exchange represents the longest-ranged and probably dominated contribution. Secondly, there exist three high-precision measurements of the $\bar{A}_L$ at different energies (Bonn at 13.6 MeV, PSI at 45 MeV, and TRIUMF at 221.3 MeV) which can be compared to the theoretical predictions. Consequently, when it comes to the one-pion exchange dominant PNC np interactions, the effect of the two-pion exchange should also be counted in.

When slow neutrons collide with hydrogen molecules, they either elastically scatter off or get absorbed in the protons resulting in deuterons and photons. This work presents calculations of the three different pion sensitive PNC observables arising from the cold neutron interaction with parahydrogen. Two are due to the PNC elastic scattering enabling the spin rotation $\frac{d}{dz}\phi$ and polarization $\frac{d}{dz}P$ of the neutrons and the third one is the γ-asymmetry $\mathcal{A}_\gamma$ in the radiative PNC capture of polarized neutrons. The spin rotation and polarization of the neutron in the PNC np scattering were first discussed in Refs. [16, 17] and the wavefunction based calculations have later been performed in Refs. [18–21]. There has also been experimental interest in measuring the PNC neutron spin rotation $\frac{d}{dz}\phi$ in a liquid parahydrogen target at the Neutron Spallation Source (SNS), see Ref. [22]. The radiative PNC reaction $\vec{n}p \to d\gamma$ is also discussed in multiple papers, of which Refs [19, 21, 23–37] present numerical predictions.

In the present work the Reid93 potential [38] is chosen to take care of the strong np interactions. The long- and medium-range parts of the weak interaction are respectively due to the one- and two- pion exchanges. The contributions of the two-pion exchanges are taken into account in the observables by using the two separate PNC NN two-pion exchange potentials taken from Refs. [39, 40]. The former of these potentials counts in the $\Delta(1232)$ isobar effects while the latter one does not. The neutron spin rotation $\frac{d}{dz}\phi$ and polarization $\frac{d}{dz}P$ are given in terms of the reduced matrix elements of the spin-space operators, which

are the basic building blocks of the PNC potentials. The radial Yukawa functions of the operators are used in unregularized form and parameterized in three different ways by the meson masses π, ρ, and ω. The calculations are performed in the distorted-wave Born approximation (DWBA), in which the phenomenological strong interaction wavefunctions sandwich the PNC operator. In the calculation of the γ-asymmetry $\mathcal{A}_\gamma$ the pion-exchange current effects are included in the form of two-body dipole operators. The required bound and continuum radial wavefunctions together with their tiny parity admixed components are obtained from the exact solution of the coupled Schrödinger equation.

The remainder of the paper is organized as follows. Section II gives the basic formalism of the cold neutron interaction with parahydrogen, Sec. III presents the results of the calculated observables, and Sec. IV summarizes the work.

II. FORMALISM

Hydrogen exists in nature in molecular form, composed of two protons bound by two electrons. The hydrogen molecule (H_2) comes in two species called parahydrogen ($H_2^{\rm p}$) and orthohydrogen ($H_2^{\rm o}$) with proton spins aligned antiparallel and parallel respectively. The de Broglie wavelength of a neutron at energies of a few meV is much greater than the internuclear separation $R_0 = 0.75$ $\mathring{A}$ between the protons in the hydrogen molecule. Consequently the neutrons, if not captured by protons, scatter coherently off the two protons in the molecules. Parahydrogen molecule is spinless, since its proton spins couple to zero and, therefore, it cannot depolarize a polarized neutron when they scatter elastically. The protonic wavefunction of the hydrogen molecule must be antisymmetric from which follows that in the ground states of the para- and orthohydrogen molecules, the rotational energies are respectively zero and $I^{-1} = 14.7$ meV, where $I = \mu R_0^2$ is the moment of inertia and μ the reduced mass of two protons. This energy determines the upper limit of the neutron center of mass (C.M.) energy in order not to get depolarized by the conversion of the para- to orthohydrogen molecule.

The low energy neutron-parahydrogen ($nH_2^{\rm p}$) interaction is a three-body problem that can crudely be simplified to a two-body neutron-proton (np) interaction problem. The np continuum wavefunctions, in which the z-axis is taken along the direction of $\boldsymbol{k}$, are of the

form

$$\langle \boldsymbol{r}|k\hat{\boldsymbol{z}};\mathcal{Q}m_n\rangle^{(\pm)} = \frac{\sqrt{4\pi}}{kr}i^L\sqrt{2L+1}\sum_{L'm_p}\langle \tfrac{1}{2}m_n\tfrac{1}{2}m_p|SM_S\rangle \times\langle L0SM_S|JM_S\rangle\mathcal{U}^{(\pm)}_{\mathcal{Q}L'}(k,r)\mathscr{Y}^{L'S}_{JM_S}(\hat{\boldsymbol{r}})(-)^{T+1}|T0\rangle, \quad (1)$$

where the superscripts $(\pm)$ refer to the incoming $(-)$ and outgoing $(+)$ wave boundary conditions, $\mathscr{Y}^{L'S}_{JM_S}(\hat{\boldsymbol{r}})$ are the eigenfunctions of the coupled angular momentum, and the quantum numbers $LSJT$ are abbreviated to $\mathcal{Q}$. The quantum numbers STJ do not change under strong interaction. Because of the antisymmetricity requirement of the wavefunction, the isospin T may as well be considered uniquely defined by the LS, and so, on occasion, the $\mathcal{Q}$ is also designated for convenience with the spectroscopic notation $\mathcal{Q} = {}^{2S+1}L_J$. An adequate deuteron wavefunction, in the γ-asymmetry $\mathcal{A}_\gamma$, is composed of three partial waves, which are the usual tensor coupled ${}^3S_1 - {}^3D_1$ and tiny parity admixed ${}^3P_1$. The np bound state wavefunction is given as

$$\langle \boldsymbol{r}|M_d\rangle = \sum_{L_d}\frac{\mathcal{D}_{L_d}(r)}{r}\mathscr{Y}^{L_d1}_{1M_d}(\hat{\boldsymbol{r}})|T_d0\rangle, \quad (2)$$

with the normalization $\int_0^\infty dr\sum_i^3|\mathcal{D}_i|^2 = 1$ and energy eigenvalue of -2.2246 MeV.

A. Neutron scattering

Since the interest here is in the coherent nH_2^p scattering, one must carefully take into account the relative motion between the neutron and system of the chemically bound protons. When a low energy neutron comes across the molecules in the medium, it interacts collectively with a number of them. As a result, the scattered waves originating from the molecules, interfere with the through passing neutron and change its momentum. Applying the Lippmann-Schwinger equation for multiple point-like scatterers each located at $\boldsymbol{r}_j$, the wave of a slow neutron after travelling through the target in the z-direction then becomes

$$e^{iq'z} \approx e^{iqz} + \tilde{f}(q,0)\sum_j\frac{e^{iq|\boldsymbol{r}-\boldsymbol{r}_j|}}{|\boldsymbol{r}-\boldsymbol{r}_j|}e^{iqz_j}, \quad (3)$$

where $\tilde{f}(q,\theta=0)$ denotes the forward nH_2^p scattering amplitude and q is the relative momentum of the neutron and molecule. The sum of the spherical waves from the scatterers in Eq. (3) may be written in the form of an integral over a smooth distribution of scattering

centers in a cylindrical shaped target of infinite radius. For the neutrons travelling along the axis of the target, it then follows that the right hand side of Eq. (3) becomes $e^{i(qz-\varphi)}$, with

$$\varphi(q,z) = -\frac{2\pi\mathcal{N}z}{q}\tilde{f}(q,0), \tag{4}$$

where $\mathcal{N}$ is the particle density of the medium. The neutron thus gains the $\varphi = (q-q')z$ amount of phase when propagating through a medium of length z. Equation (4) is related to the index of refraction $n = q'/q = 1 - \varphi/qz$ in neutron optics.

By the initial choice of the transversely polarized spin in the positive x-direction $\langle\sigma_x\rangle = +1$, the neutron spin wavefunction $|x+\rangle = (|+\rangle + |-\rangle)/\sqrt{2}$ contains equal amount of $\pm$ helicities in the direction of its propagation along the z-axis. The PNC interaction favors one helicity state slightly more than the other and thus depending on this state, the neutrons scatter a bit differently. The neutron wavefunction accumulates the φ_{m_n} amount phase (where m_n is the spin polarization of the incident neutron) labeled individually for each two states when passing through the target. It follows straightforwardly from the expectation value of the spin $\langle\boldsymbol{\sigma}\rangle$, that the neutron spin rotates in the xy-plane around the z-axis if the real value of the subtraction between the helicity states of Eq. (4) is non-zero

$$\phi(q,z) = -\frac{2\pi\mathcal{N}z}{q}\mathrm{Re}\Big(\tilde{f}_{+\frac{1}{2}}(q,0) - \tilde{f}_{-\frac{1}{2}}(q,0)\Big). \tag{5}$$

In the case of the unpolarized neutron beam, the neutrons gain some amount of longitudinal polarization due to the parity nonconservation when propagating through a medium. The incident beam intensity loss is given by $dI_\pm(q,z) = -\mathcal{N}\sigma_\pm(q)I_\pm(q,z)dz$ from which, with the help of the optical theorem, the fractional polarization follows as the difference between the $I_+(q,z)$ and $I_-(q,z)$ divided by their sum

$$P(q,z) \approx -\frac{2\pi\mathcal{N}z}{q}\mathrm{Im}\Big(\tilde{f}_{+\frac{1}{2}}(q,0) - \tilde{f}_{-\frac{1}{2}}(q,0)\Big). \tag{6}$$

The nH_2^p scattering amplitude may be written as $\tilde{f} = -(\tilde{\mu}/\mu)\tilde{a}$ in which the $\mu \approx M/2$ and $\tilde{\mu} \approx 2M/3$ are respectively the neutron-proton and neutron-molecule reduced masses with the average nucleon mass $M = 939$ MeV and $\tilde{a} = (a_s + 3a_t)/2$ (see *e.g.* Ref. [41]) is the coherent scattering length expressed in terms of the np scattering lengths for the singlet ${}^1S_0$ and triplet ${}^3S_1$ channels. That is $\tilde{a} = -f/2$, where f is the np scattering amplitude. The nH_2^p and np scattering amplitudes and momenta are related as $\tilde{f} = (\tilde{\mu}/2\mu)f$ and $q = (\tilde{\mu}/\mu)k$, where k is the relative momentum of the neutron and proton. The relevant PNC part of

the forward np scattering amplitude $f_{m_n}(k,\theta=0)$ in distorted wave Born approximation (DWBA) is given by

$$f_{m_n}(k,0) = -\frac{\mu}{2\pi}{}^{(-)}\langle k\hat{\boldsymbol{z}}; m_n|\hat{V}^{\rm PNC}|k\hat{\boldsymbol{z}}; m_n\rangle^{(+)}, \tag{7}$$

where the matrix elements are Hermitian. The $S \leftrightarrow P$ transitions are sufficient in the low energy PNC scattering and also equally important in both ways. Considering the lowest amplitudes, the derivative of the common factor in Eqs. (5) $\frac{d}{dz}\phi = {\rm Re}\mathcal{O}(k)$ and (6) $\frac{d}{dz}P = {\rm Im}\mathcal{O}(k)$ (both per unit length) becomes

$$\mathcal{O}(k) = \frac{2i\pi M\mathcal{N}}{k^3}\Big(\mathcal{W}^{^3P_0}_{^1S_0}(k) - \sqrt{2}\mathcal{W}^{^3P_1}_{^3S_1}(k) - \mathcal{W}^{^1P_1}_{^3S_1}(k)\Big), \tag{8}$$

where the subscript $^3S_1$ includes also its tensor coupled partner, the $^3D_1$ partial wave. The matrix elements of the PNC potential are further written in terms of the matrix elements of the operators, which appear in the PNC potentials of the DDH model and EFT, as

$$\mathcal{W}^{^3P_0}_{^1S_0}(k) = \frac{1}{M}\sum_\alpha\Big(\mathcal{C}^{1\alpha}_{1[\times]_-}\mathcal{J}^{^3P_0\alpha}_{^1S_0[\times]_-}(k) + \mathcal{C}^{1\alpha}_{1[-]_+}\mathcal{J}^{^3P_0\alpha}_{^1S_0[-]_+}(k)\Big), \tag{9}$$

$$\mathcal{W}^{^3P_1}_{^3S_1}(k) = \frac{1}{M}\Big(\mathcal{C}^{1\pi}_{0[+]_-}\mathcal{J}^{^3P_1\pi}_{^3S_1[+]_-}(k) + \sum_\alpha\mathcal{C}^{1\alpha}_{0[+]_+}\mathcal{J}^{^3P_1\alpha}_{^3S_1[+]_+}(k)\Big), \tag{10}$$

$$\mathcal{W}^{^1P_1}_{^3S_1}(k) = \frac{1}{M}\sum_\alpha\Big(\mathcal{C}^{0\alpha}_{0[\times]_-}\mathcal{J}^{^1P_1\alpha}_{^3S_1[\times]_-}(k) + \mathcal{C}^{0\alpha}_{0[-]_+}\mathcal{J}^{^1P_1\alpha}_{^3S_1[-]_+}(k)\Big), \tag{11}$$

where the meson label α $(=\rho,\omega)$ is for the DDH model. In the case of EFT the α's and summation symbols are omitted. The reduced matrix elements of the spin-space operators

$$\mathcal{J}^{\mathcal{Q}'\alpha}_{\mathcal{Q}[\odot]_\pm}(k) = {}^{(-)}\langle k\hat{\boldsymbol{z}}; \mathcal{Q}'||(\boldsymbol{\sigma}_1\odot\boldsymbol{\sigma}_2)\cdot[-i\boldsymbol{\nabla}, Y_\alpha(r)]_\pm||k\hat{\boldsymbol{z}}; \mathcal{Q}\rangle^{(+)}, \tag{12}$$

with $(\odot = \pm, \times)$ are separated into the commutator $[\odot]_-$ and anticommutator $[\odot]_+$ elements. The constants $\mathcal{C}^{T'\alpha}_{T[\odot]_\pm}$, where T denotes the total isospin in the initial and T' in the final state, include the matrix elements of the isospin operators and the other parameters associated with the potential, *e.g.* in the case of the DDH and pion, the constant is $\mathcal{C}^{1\pi}_{0[+]_-} = g_\pi h^{(1)}_\pi/\sqrt{2}$.

B. Neutron capture

The thermal neutron capture cross-section on molecular hydrogen does not depend on the interference or binding effects of the protons in the molecule [42]. It is therefore sufficient to

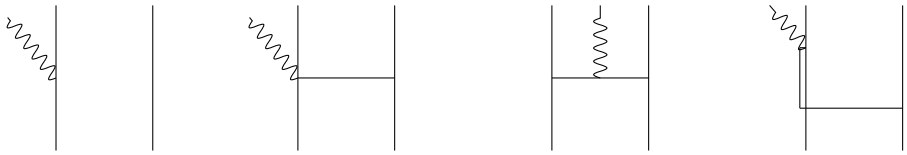

FIG. 1. The diagrams for the magnetic dipole moments considered in the calculation of $\sigma(np \to \gamma d)$. From left to right they are called impulse (imp), seagull (sea), pion-in-flight (fly), and delta (Δ) diagram. The wavy line is a photon, the solid line is a nucleon, the dashed line is a pion, and the bar is a Δ-isobar.

simply calculate the neutron capture cross-section on free protons. The M1 ${}^1S_0 \to {}^3S_1 - {}^3D_1$ transition dominates the $np \to \gamma d$ reaction at threshold. By far the largest contribution (of about 90 %) of this reaction arises from the impulse approximation which couples the S-states. However, the one-pion exchange currents can also reach the D-state of the deuteron and play an important role in explaining the experimental value of the cross-section for thermal neutrons as was shown in Ref. [43].

The relevant photoproduction vertices, in terms of Lagrangian densities, are for the $\gamma NN\pi$ interaction

$$\mathscr{L}_{\gamma NN\pi} = -e\frac{f_\pi}{m_\pi}\bar{N}\gamma_5\gamma^\mu(\boldsymbol{\tau}\times\boldsymbol{\pi})_z N A_\mu \tag{13}$$

and for the $\gamma\pi\pi$ interaction

$$\mathscr{L}_{\gamma\pi\pi} = -e(\partial^\mu\boldsymbol{\pi}\times\boldsymbol{\pi})_z A_\mu. \tag{14}$$

Since the energy of the resulting photon at threshold of the reaction is only about 2 MeV, its wavelength is much larger than the deuteron size, and thus the electric $\boldsymbol{E}$ and magnetic $\boldsymbol{B}$ fields can be taken as constants. The scalar and vector potentials of the uniform (static) fields $\boldsymbol{E}$ and $\boldsymbol{B}$ are $\phi(\boldsymbol{r}) = -\boldsymbol{E}\cdot\boldsymbol{r}$ and $\boldsymbol{A}(\boldsymbol{r}) = \frac{1}{2}\boldsymbol{B}\times\boldsymbol{r}$ respectively.

A diagrammatic illustration for the one- and two-body magnetic dipole moment operators is given in Fig. 1. Besides Eqs. (13) and (14), the other necessary $\gamma N\Delta$, $\pi N\Delta$, and (PC and PNC) πNN Lagrangians are given (in nonrelativistic form) in Appendix A. In the impulse approximation, the relevant spin changing part of the operator is

$$\hat{\boldsymbol{m}}^{\rm imp} = \frac{\mu_v}{4}(\hat{\tau}_{1z} - \hat{\tau}_{2z})(\boldsymbol{\sigma}_1 - \boldsymbol{\sigma}_2). \tag{15}$$

The seagull contribution follows from Eqs. (13) and (A1) leading to the exchange operator

$$\hat{\boldsymbol{m}}^{\rm sea}(\boldsymbol{r}) = -\frac{M}{2}\Big(\frac{f_\pi}{m_\pi}\Big)^2(\boldsymbol{\tau}_1\times\boldsymbol{\tau}_2)_z\Big\{\hat{\boldsymbol{r}}[\hat{\boldsymbol{r}}\cdot(\boldsymbol{\sigma}_1\times\boldsymbol{\sigma}_2)] - \boldsymbol{\sigma}_1\times\boldsymbol{\sigma}_2\Big\}(1+m_\pi r)\frac{e^{-m_\pi r}}{4\pi r}. \tag{16}$$

Similarly, the pion-in-flight contribution (the Sachs exchange moment) is given by Eqs. (14) and (A1)

$$\hat{\boldsymbol{m}}^{\rm fly}(\boldsymbol{r}) = \\ -\frac{M}{2}\Big(\frac{f_\pi}{m_\pi}\Big)^2(\boldsymbol{\tau}_1\times\boldsymbol{\tau}_2)_z\Big\{\hat{\boldsymbol{r}}[\hat{\boldsymbol{r}}\cdot(\boldsymbol{\sigma}_1\times\boldsymbol{\sigma}_2)](1+m_\pi r)+\boldsymbol{\sigma}_1\times\boldsymbol{\sigma}_2(1-m_\pi r)\Big\}\frac{e^{-m_\pi r}}{4\pi r}. \quad (17)$$

The final correction becomes by taking into account the static $N\Delta$ intermediate state by using Eqs. (A1), (A2), and (A3)

$$\hat{\boldsymbol{m}}^{\Delta}(\boldsymbol{r}) = \frac{\mu_\Delta f_\pi^\star f_\pi}{9(M_\Delta - M)}\Big((\hat{\tau}_{1z}-\hat{\tau}_{2z})-i(\boldsymbol{\tau}_1\times\boldsymbol{\tau}_2)_z\Big)\Big\{i(\boldsymbol{\sigma}_1\times\hat{\boldsymbol{r}})(\boldsymbol{\sigma}_2\cdot\hat{\boldsymbol{r}}) \\ -i(\boldsymbol{\sigma}_2\times\hat{\boldsymbol{r}})(\boldsymbol{\sigma}_1\cdot\hat{\boldsymbol{r}})-2(\boldsymbol{\sigma}_1-\boldsymbol{\sigma}_2)\cdot\hat{\boldsymbol{r}}\hat{\boldsymbol{r}}\Big\}\Big(1+\frac{3}{m_\pi r}+\frac{3}{(m_\pi r)^2}\Big)\frac{e^{-m_\pi r}}{4\pi r}, \quad (18)$$

where the irrelevant isospin conserving terms are omitted as in the case of $\hat{\boldsymbol{m}}^{\rm imp}$. The total magnetic moment operator is given by $\hat{\boldsymbol{m}} = \hat{\boldsymbol{m}}^{\rm imp}+\hat{\boldsymbol{m}}^{\rm sea}+\hat{\boldsymbol{m}}^{\rm fly}+\hat{\boldsymbol{m}}^{\Delta}$.

The nonzero γ-asymmetry $\mathcal{A}_\gamma$ arises from the interference between the M1 transition and the PNC interaction propelled E1 transitions. The E1 transitions connect the initial ${}^3S_1-{}^3D_1$ and final deuteron states through the parity admixed continuum and bound $\widetilde{{}^3P_1}$ states, while the PNC E1 transitions connect them directly. Figure 2 gives the diagrams for electric dipole moment contributions. The one-body operator is given by

$$\hat{\boldsymbol{\mu}}_e^{\rm imp} = \frac{e}{4}(\hat{\tau}_{1z}-\hat{\tau}_{2z})\boldsymbol{r} \quad (19)$$

and the two-body PNC exchange operator results from Eqs. (13) and (A4)

$$\hat{\boldsymbol{\mu}}_e^{\rm PNC}(\boldsymbol{r}) = \frac{e}{4M}\frac{f_\pi h_\pi^{(1)}}{m_\pi\sqrt{2}}(\boldsymbol{\tau}_1\cdot\boldsymbol{\tau}_2-\hat{\tau}_{1z}\hat{\tau}_{2z})\Big[i(\boldsymbol{\sigma}_1+\boldsymbol{\sigma}_2)\frac{e^{-m_\pi r}}{4\pi r}-\boldsymbol{r}(\boldsymbol{\sigma}_1+\boldsymbol{\sigma}_2)\cdot\Big\{-i\boldsymbol{\nabla},\frac{e^{-m_\pi r}}{4\pi r}\Big\}\Big]. \quad (20)$$

The total E1 operator is the sum $\hat{\boldsymbol{\mu}}_e = \hat{\boldsymbol{\mu}}_e^{\rm imp}+\hat{\boldsymbol{\mu}}_e^{\rm PNC}$. Note that the $\hat{\boldsymbol{\mu}}_e^{\rm imp}$ changes parity, while the $\hat{\boldsymbol{\mu}}_e^{\rm PNC}$ conserves it. Reference [44] investigates the PNC E1 transitions and gives an additional $\gamma NN\pi$ vertex leading to the spin-changing PNC E1 operator. However, this vertex has a vanishing contribution to the $\mathcal{A}_\gamma$ because the term proportional to the $\boldsymbol{B}$ is negligibly small and the M1-E1 interference disappears as a consequence of the initial ${}^1S_0$ states in both amplitudes.

In terms of the reduced matrix elements of the electric and magnetic dipole transition operators, the γ-asymmetry $\mathcal{A}_\gamma = (d\sigma_{+\frac{1}{2}}-d\sigma_{-\frac{1}{2}})/(d\sigma_{+\frac{1}{2}}+d\sigma_{-\frac{1}{2}})$ reads now

$$\mathcal{A}_\gamma(k) = \sqrt{2}{\rm Re}\Big[\frac{i\sum_{LL^d}\int_0^\infty dr\mathcal{D}_{L^d}(r)\langle{}^3L_1^d||\hat{\boldsymbol{\mu}}_e(\boldsymbol{r})||{}^3L_1\rangle\mathcal{U}^{(+)}_{{}^3L_1}(r,k)}{\sum_{L^d}\int_0^\infty dr\mathcal{D}_{L^d}(r)\langle{}^3L_1^d||\hat{\boldsymbol{\mu}}_m(\boldsymbol{r})||{}^1S_0\rangle\mathcal{U}^{(+)}_{{}^1S_0}(r,k)}\Big], \quad (21)$$

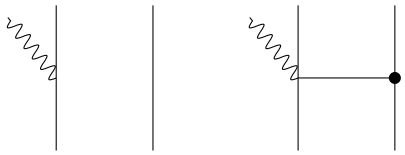

FIG. 2. The E1 contributions to the γ-asymmetry $\mathcal{A}_\gamma$. The black dot denotes the parity nonconserving vertex.

where $\hat{\boldsymbol{\mu}}_m = e\hat{\boldsymbol{m}}/2M$ and the multiplication factor $\cos\theta$, in which θ is the angle between the neutron spin and photon direction, is left out.

III. RESULTS

The results for the neutron spin rotation $\frac{d}{dz}\phi$, polarization $\frac{d}{dz}P$, and γ-asymmetry $\mathcal{A}_\gamma$ are given in this section. The NN wavefunctions are the exact solutions of the coupled Schrödinger equations where the strong distortions originate from the Reid93 potential [38]. The OME parts of the observables can be and are, as customary, evaluated without regularization. The $\frac{d}{dz}\phi$ and $\frac{d}{dz}P$ are low energy scattering problems which are handled perturbatively within the DWBA and therefore the inclusion of the form factors is not crucial. The DWBA approach allows the PNC potentials to be omitted from the Schrödinger equations because of their diminutive distortive effects to the strong wavefunctions. This, however, is not possible in the calculation of the $\mathcal{A}_\gamma$ since the parity admixed wavefunctions are needed. In this case also the regularization of the PNC TPE potentials becomes necessity for the reason that they are too singular to be treated without it. As for the DDH model results, the DDH "best" values for the weak couplings are used along with the strong couplings $g_\pi = 13.45$, $g_\rho = 2.79$, and $g_\omega = 8.37$ and the anomalies $\chi_\rho = 3.71$ and $\chi_\omega = -0.12$.

The employed TPE potentials are taken from Refs. [39] and [40] and respectively abbreviated as $\hat{V}_{\rm K}^{\rm TPE}(\boldsymbol{r})$ and $\hat{V}_{\rm D}^{\rm TPE}(\boldsymbol{r})$ of which the former takes into account the NN and $N\Delta$ intermediate states while the latter only the NN. The NN intermediate parts of these potentials coincide, if the constant term in the dispersion relation of the $\hat{V}_{\rm D}^{\rm TPE}(\boldsymbol{r})$ is excluded. The constant term in momentum space corresponds to a term proportional to the delta function $\delta(\boldsymbol{r})$ in coordinate space. However, when the TPE potentials are regularized by form factors, their NN parts inevitably differ from each other. The TPE potentials are modified by the monopole $\Lambda^2(\boldsymbol{q}^2+\Lambda^2)^{-1}$ and dipole $\Lambda^4(\boldsymbol{q}^2+\Lambda^2)^{-2}$ form factors and used

with three different cut-off mass values $\Lambda = 0.8$, 1.0, and 1.2 GeV. The same type of the monopole form factor emerged with the PNC TPE potential $\hat{V}_{\rm D}^{\rm TPE}(\boldsymbol{r})$ was also used in Ref. [34] to calculate the γ-asymmetry in $\vec{n}p \to \gamma d$ at threshold. The results of the medium-range TPE are sensitive to the form factors, which have an increasingly suppressing effect on them when the cut-off is decreased and the rank of the form factor is raised.

A. Neutron spin rotation $\frac{d}{dz}\phi$ and polarization $\frac{d}{dz}P$

The spin-space operators appearing in Eq. (12) are common building blocks in the PNC NN interaction. In the approach in which the operators are placed between high-quality phenomenological wavefunctions, the low-energy $\lesssim 1$ keV scattering matrix elements can be expressed in constant form, as given in Tab. I. Therefore, by means of the matrix elements of Tab. I, it is straightforward to customize the OME contributions within any model that uses the π, ω, and/or ρ exchanges as the ranges of the unmodified Yukawa functions $Y_\alpha(r) = e^{-m_\alpha r}/4\pi r$.

The neutron spin rotation is split into one-meson exchange (OME) and two-pion exchange (TPE) components as $\frac{d}{dz}\phi = \frac{d}{dz}\phi^{\rm OME} + \frac{d}{dz}\phi^{\rm TPE}$. Since a neutron scatters coherently from a

TABLE I. The values of Eq. (12) for the spin rotation components $\mathcal{I}^{\mathcal{Q}'\alpha}_{\mathcal{Q}[\times]_-}(k) = {\rm Re}\Big(k^{-3}\mathcal{J}^{\mathcal{Q}'\alpha}_{\mathcal{Q}[\times]_-}(k)\Big)$ and $\mathcal{I}^{\mathcal{Q}'\alpha}_{\mathcal{Q}[\pm]_\pm}(k) = {\rm Re}\Big(-ik^{-3}\mathcal{J}^{\mathcal{Q}'\alpha}_{\mathcal{Q}[\pm]_\pm}(k)\Big)$ in units of mb and for the spin polarization components $\mathcal{G}^{\mathcal{Q}'\alpha}_{\mathcal{Q}[\times]_-}(k) = \frac{k}{T^n_{\rm Lab}}{\rm Im}\Big(k^{-3}\mathcal{J}^{\mathcal{Q}'\alpha}_{\mathcal{Q}[\times]_-}(k)\Big)$ and $\mathcal{G}^{\mathcal{Q}'\alpha}_{\mathcal{Q}[\pm]_\pm}(k) = \frac{k}{T^n_{\rm Lab}}{\rm Im}\Big(-ik^{-3}\mathcal{J}^{\mathcal{Q}'\alpha}_{\mathcal{Q}[\pm]_\pm}(k)\Big)$ in units of 10^{-10} fm/meV. The k and $T^n_{\rm Lab}$ (related as $T^n_{\rm Lab} = \frac{2k^2}{M}$) are respectively in units of fm^{-1} and meV. The functions $\mathcal{I}$ and $\mathcal{G}$ are constants within the neutron kinetic energy range of about $T^n_{\rm Lab}$=0-1 keV.

	π	ρ	ω
$\mathcal{I}^{^3P_0\alpha}_{^1S_0[\times]_-}$	-30.1992	-0.7825	-0.7444
$\mathcal{I}^{^3P_0\alpha}_{^1S_0[-]_+}$	-42.2133	-0.6494	-0.6143
$\mathcal{I}^{^1P_1\alpha}_{^3S_1[\times]_-}$	1.5588	0.0868	0.0834
$\mathcal{I}^{^1P_1\alpha}_{^3S_1[-]_+}$	-4.4409	-0.1020	-0.0975
$\mathcal{I}^{^3P_1\alpha}_{^3S_1[+]_-}$	3.4753	0.1528	0.1459
$\mathcal{I}^{^3P_1\alpha}_{^3S_1[+]_+}$	5.6818	0.0843	0.0798

	π	ρ	ω
$\mathcal{G}^{^3P_0\alpha}_{^1S_0[\times]_-}$	-8.6220	-0.2234	-0.2125
$\mathcal{G}^{^3P_0\alpha}_{^1S_0[-]_+}$	-12.0522	-0.1854	-0.1754
$\mathcal{G}^{^1P_1\alpha}_{^3S_1[\times]_-}$	-0.1020	-0.0057	-0.0055
$\mathcal{G}^{^1P_1\alpha}_{^3S_1[-]_+}$	0.2905	0.0067	0.0064
$\mathcal{G}^{^3P_1\alpha}_{^3S_1[+]_-}$	-0.2273	-0.0100	-0.0095
$\mathcal{G}^{^3P_1\alpha}_{^3S_1[+]_+}$	-0.3717	-0.0055	-0.0052

pair of protons in the hydrogen molecule, it is then appropriate to use the molecule number density of liquid hydrogen instead of a two times larger atom number density. Therefore, the liquid parahydrogen particle density value of $\mathcal{N} = 0.021$ molecules/$\mathring{A}^3$ is used in the numerical results. In terms of the DDH model, the rotation may be written as

$$\frac{d}{dz}\phi^{\rm OME}_{\rm DDH} = \Big(0.617h^{(1)}_\pi - 0.138h^{(0)}_\omega - 0.012h^{(1)}_\omega - 0.126h^{(0)}_\rho + 0.004h^{(1)}_\rho + 0.130h^{(2)}_\rho\Big)\frac{\rm rad}{\rm m}. \quad (22)$$

This has the value of 3.31×10^{-7} $\frac{\rm rad}{\rm m}$ when the DDH "best" values are plugged in. With this model and values, the one-pion exchange (OPE) has a dominance of about 85%. The result of Eq. (22) is consistent with the one in Ref. [20], except half the size (because of the half the size particle density value), and also in line with the predictions of Refs. [19, 21] which all employ the Argonne v_{18} potential. The result using the Paris potential reported in Ref. [18] is in the same order with the aforementioned results but of the opposite sign. Also in the result of Ref. [18] some of the signs between the partial contributions are in disagreement with the mutually consistent results of Ref. [20] and Eq. (22).

TABLE II. The TPE contributions to the neutron spin rotation $\frac{d}{dz}\phi^{\rm TPE}$ in units of $h^{(1)}_\pi \frac{\rm rad}{\rm m}$ and polarization $\frac{k}{T^n_{\rm Lab}}\frac{d}{dz}P^{\rm TPE}$ in units of $h^{(1)}_\pi \times 10^{-12}$ fm^{-1}m^{-1}meV^{-1}. The K and D stand for the $\hat{V}^{\rm TPE}_{\rm K}(\boldsymbol{r})$ and $\hat{V}^{\rm TPE}_{\rm D}(\boldsymbol{r})$ while the F and FF stand respectively for the modification by $\Lambda^2(\boldsymbol{q}^2+\Lambda^2)^{-1}$ and $\Lambda^4(\boldsymbol{q}^2+\Lambda^2)^{-2}$, where the cut-off masses Λ are in units of GeV.

$\frac{d}{dz}\phi^{\rm TPE}$				
Λ	K(FF)	D(FF)	K(F)	D(F)
0.8	−0.040	0.026	−0.105	−0.020
1.0	−0.074	0.004	−0.132	−0.040
1.2	−0.103	−0.017	−0.152	−0.055

$\frac{k}{T^n_{\rm Lab}}\frac{d}{dz}P^{\rm TPE}$				
Λ	K(FF)	D(FF)	K(F)	D(F)
0.8	2.648	−1.712	6.845	1.295
1.0	4.844	−2.442	8.648	2.619
1.2	6.763	1.104	9.925	3.604

Because the $\hat{V}^{\rm TPE}_{\rm D}(\boldsymbol{r})$ and NN part of the $\hat{V}^{\rm TPE}_{\rm K}(\boldsymbol{r})$ are identical in unregularized form, they contribute the same amount to the rotation $\frac{d}{dz}\phi^{\rm TPE}_{NN} = -0.101h^{(1)}_\pi$ $\frac{\rm rad}{\rm m}$ reducing the OPE effect by about 15%. By taking into account also the Δ effects of the $\hat{V}^{\rm TPE}_{\rm K}(\boldsymbol{r})$, the contribution doubles to $\frac{d}{dz}\phi^{\rm TPE}_{\rm K} = -0.209h^{(1)}_\pi$ $\frac{\rm rad}{\rm m}$ cutting down the OPE effect by over 30%. However, since the TPE is a medium-range effect, it is sensitive to form factors. The form factor modified TPE contributions to the $\frac{d}{dz}\phi^{\rm TPE}$ are given in Tab. II. As is seen in the Table, the regularized TPE contributions are, like the unregularized ones, negative in almost all

cases and, thus, opposite to the OPE effect. Only the D(FF) case differs by having a different sign at small cut-off masses.

When it comes to the neutron spin polarization $\frac{d}{dz}P$, the effect is much smaller than the one of $\frac{d}{dz}\phi$ and therefore not particularly interesting because it is experimentally much less achievable. For example, similarly to Eq. (22), the DDH OME contribution to the polarization with $T^n_{\rm Lab} = 10$ meV neutrons is only $\frac{d}{dz}P^{\rm OME}_{\rm DDH} = 7.43 \times 10^{-12}\ \frac{1}{m}$. This result can be constructed by using the matrix elements $\mathcal{G}^{\mathcal{Q}'\alpha}_{\mathcal{Q}[\odot]_\pm}(k)$ of Tab. I, which lead with the DDH "best" values to $\frac{k}{T^n_{\rm Lab}}\frac{d}{dz}P^{\rm OME}_{\rm DDH} = 8.17 \times 10^{-18}$ fm^{-1}m^{-1}meV^{-1}. The OPE contribution to this number in the same units is -18.54 and has, thus, about 70% dominance. As in the rotation, the unregularized TPE contributions to the $\frac{k}{T^n_{\rm Lab}}\frac{d}{dz}P^{\rm TPE}$ (in units of $h^{(1)}_\pi \times 10^{-12}$ fm^{-1}m^{-1}meV^{-1}) are 6.63 and 13.70, in which the former is the same for both potentials when only the NN intermediate states are considered and the latter is for the $\hat{V}^{\rm TPE}_{\rm K}(\boldsymbol{r})$ when also the $N\Delta$ intermediate states are included. As in the corresponding case of the rotation, the TPE effect with the Δ, diminish over 30% the OPE contribution. The effects of the form factors on the $\frac{k}{T^n_{\rm Lab}}\frac{d}{dz}P^{\rm TPE}$ are presented in Tab. II and show similar features as in the case of the spin rotation.

B. Photon asymmetry $\mathcal{A}_\gamma$

An experimental value of the radiative thermal neutron capture cross-section of proton is $\sigma(np \to \gamma d) = 334.2 \pm 0.5$ mb [45]. Theoretically it may be given by

$$\sigma_{\rm cap} = \frac{\alpha\pi\omega^3_\gamma}{6k^3M}\sum_{L_d}\Big|\int_0^\infty dr\mathcal{D}_{L_d}(r)\langle {}^3L_{d1}||\hat{\boldsymbol{m}}(\boldsymbol{r})||{}^1S_0\rangle\mathcal{U}^{(+)}_{{}^1S_0}(r,k)\Big|^2, \tag{23}$$

where $\alpha\ (= e^2)$ is the fine structure constant, ω_γ the C.M. energy of the photon, and $\hat{\boldsymbol{m}}(\boldsymbol{r})$ the magnetic moment operator, which is the sum of Eqs. (15)-(18). The used coupling values are $g_\pi = 13.45$ ($f_\pi = m_\pi g_\pi/2M$), $f^\star_\pi = \sqrt{72/25}f_\pi$, and $\mu_\Delta = f^\star_\pi\mu_v/2f_\pi$ ($f_{\gamma N\Delta}/m_\pi = e\mu_\Delta/2M$), where g_π is the πNN coupling, $f^\star_\pi$ the quark model result for the $\pi N\Delta$ coupling [46], μ_Δ the transition magnetic moment, and $\mu_v = 4.71$ the isovector magnetic moment of the nucleon. Evaluation of Eq. (23) for the thermal neutrons ($T^n_{\rm Lab} = 25$ meV) gives $\sigma_{\rm cap} = 334.42$ mb, which is in an excellent agreement with the experimental cross-section. In this result, the mere impulse approximation, *i.e.* $\hat{\boldsymbol{m}}(\boldsymbol{r}) = \hat{\boldsymbol{m}}^{\rm imp}$, produces the largest part of the cross-section giving $\sigma^{\rm imp}_{\rm cap} = 303.81$ mb. The missing $\sim 10\%$ enhancement results from the OPE

current corrections, as proposed in Ref. [43].

By using the DDH model and their "best" coupling values, the OME contribution to the γ-asymmetry Eq. (21) is $\mathcal{A}_{\gamma\mathrm{DDH}}^{\mathrm{OME}} = -5.387 \times 10^{-8}$. Even though included, the effects of the PNC E1 current ($\sim -0.2‰$) and heavy meson ρ- and ω-exchanges (less than 1%) are negligibly small. In terms of the weak pion coupling, the result may be written as $\mathcal{A}_{\gamma\mathrm{DDH}}^{\mathrm{OME}} \approx -0.117 h_\pi^{(1)}$ which is in harmony with the previous predictions (see the references mentioned in the Introduction) in most cases. The results, in which the TPE contributions are added on top of the $\mathcal{A}_{\gamma\mathrm{DDH}}^{\mathrm{OME}}$, are shown in Tab. III and are rather self-explaining. The result of the model D(F) with $\Lambda = 1.0$ GeV is consistent with Ref. [34] and show $\sim 6\%$ smaller γ-asymmetry than without the TPE. Just like in scattering cases, the TPE contribution of the D(FF) model with $\Lambda = 0.8$ and 1.0 GeV differs by the sign from the other models and, therefore, strengthens the total asymmetry. Otherwise the TPE effect is destructive as in the case of the $\frac{d}{dz}\phi^{\mathrm{TPE}}$. The largest contribution arises from the K(F) model with $\Lambda = 1.2$ GeV, which diminishes the $\mathcal{A}_{\gamma\mathrm{DDH}}^{\mathrm{OME}}$ of about about 20%.

TABLE III. Photon asymmetry $\mathcal{A}_\gamma$ including the TPE in units of 10^{-8}.

$\mathcal{A}_\gamma(\vec{n}p \to \gamma d)$				
Λ	K(FF)	D(FF)	K(F)	D(F)
0.8	−5.08	−5.58	−4.60	−5.24
1.0	−4.83	−5.41	−4.40	−5.08
1.2	−4.61	−5.26	−4.26	−4.97

IV. SUMMARY

Three PNC observables for cold neutron interaction with parahydrogen were calculated. All the observables, the neutron spin rotation $\frac{d}{dz}\phi$ and polarization $\frac{d}{dz}P$ in scattering, and the γ-asymmetry $\mathcal{A}_\gamma$ in capture, were found to be dominated by the pion exchange. The effect of the TPE was also taken into account in these observables and investigated in several settings. In all cases, the TPE effect was mainly opposite to the one of the OPE.

The OME contribution to the $\frac{d}{dz}\phi$ was concluded to be a factor of two smaller than the most recent predictions and that the TPE decreased it up to $\sim 30\%$ further. The $\frac{d}{dz}P$ was

considered rather uninteresting due to its small size. In the $\mathcal{A}_\gamma$, the OPE currents gave the expected increment for the M1 transitions but were insignificant for PNC E1 ones. The asymmetry was found to arise more or less completely from the pion exchange, *i.e.* the OPE weakened by the TPE up to $\sim 20\%$ or so.

Unfortunately, so far there exist no direct and helpful experimental data for these specific observables. However, as already mentioned, there exist three precision experiment data points of the PNC longitudinal analyzing power $\bar{A}_L(\vec{p}p \to pp)$ of which two are low energy points originating completely from the ${}^1S_0 - {}^3P_0$ transition. A recent $\bar{A}_L$ calculation of Ref. [14] uses exactly the same TPE models (potentials, couplings, and form factors) as used here. Based on the DDH model along with the TPE model K(FF) with $\Lambda = 1.0$ GeV gives the best fit and is also in a good agreement with the experimental data. This suggests that, in the calculated observables $\frac{d}{dz}\phi$, $\frac{d}{dz}P$, and $\mathcal{A}_\gamma$, the destructive TPE effect compared to the OPE one is roughly 10% in each case.

ACKNOWLEDGMENTS

The author is grateful to Dr. J. A. Niskanen for advice and reading the manuscript. The financial support from Vilho, Yrjö ja Kalle Väisälä Foundation is also gratefully acknowledged.

Appendix A

The nonrelativistic interaction Lagrangians (the couplings are explained in the text) are

$$L_{\pi NN} = \frac{f_\pi}{m_\pi} \boldsymbol{\sigma} \cdot \boldsymbol{\nabla} \boldsymbol{\tau} \cdot \boldsymbol{\pi}, \tag{A1}$$

$$L_{\gamma N\Delta} = \frac{f_{\gamma N\Delta}}{m_\pi} \boldsymbol{S} \cdot \boldsymbol{B} \hat{T}_z + \text{H.c.}, \tag{A2}$$

$$L_{\pi N\Delta} = \frac{f_\pi^\star}{m_\pi} \boldsymbol{S} \cdot \boldsymbol{\nabla} \boldsymbol{T} \cdot \boldsymbol{\pi} + \text{H.c.}, \tag{A3}$$

$$L_{\pi NN}^{\text{PNC}} = \frac{h_\pi^{(1)}}{\sqrt{2}} (\boldsymbol{\tau} \times \boldsymbol{\pi})_z. \tag{A4}$$

The $\boldsymbol{S}$ and $\boldsymbol{T}$ are respectively the $N\Delta$ spin and isospin transition operators [46].

[1] S.-L. Zhu, C. M. Maekawa, B. R. Holstein, M. J. Ramsey-Musolf, and U. van Kolck, Nucl. Phys. **A748**, 435 (2005)

[2] M. J. Ramsey-Musolf and S. A. Page, Ann. Rev. Nucl. Part. Sci. **56**, 1 (2006)

[3] B. Desplanques, J. F. Donoghue, and B. R. Holstein, Ann. Phys. (N.Y.) **124**, 449 (1980)

[4] G. B. Feldman, G. A. Crawford, J. Dubach, and B. R. Holstein, Phys. Rev. **C43**, 863 (1991)

[5] B. Desplanques, Nucl. Phys. **A335**, 147 (1980)

[6] V. M. Dubovik and S. V. Zenkin, Annals Phys. **172**, 100 (1986)

[7] M. J. Iqbal and J. A. Niskanen, Phys. Rev. **C42**, 1872 (1990)

[8] N. Kaiser and U. G. Meissner, Nucl. Phys. **A499**, 699 (1989)

[9] E. M. Henley, W. Y. P. Hwang, and L. S. Kisslinger, Phys. Lett. **B440**, 449 (1998)

[10] G. A. Lobov, Phys. Atom. Nucl. **65**, 534 (2002)

[11] H.-J. Lee, C. H. Hyun, and H.-C. Kim(2012), arXiv:1203.4769 [hep-ph]

[12] M. T. Gericke *et al.*, Phys. Rev. **C83**, 015505 (2011)

[13] J. A. Niskanen, T. M. Partanen, and M. J. Iqbal, Eur. Phys. J. **A36**, 295 (2008)

[14] T. M. Partanen, J. A. Niskanen, and M. J. Iqbal(2012), arXiv:1204.0434 [nucl-th]

[15] G. Barton, Nuovo Cimento **19**, 512 (1961)

[16] F. C. Michel, Phys. Rev. **133**, B329 (1964)

[17] L. Stodolsky, Phys. Lett. **B50**, 352 (1974)

[18] Y. Avishai and P. Grange, J. Phys. **G10**, L263 (1984)

[19] R. Schiavilla, J. Carlson, and M. W. Paris, Phys. Rev. **C70**, 044007 (2004)

[20] C.-P. Liu and R. G. E. Timmermans, Phys. Lett. **B634**, 488 (2006)

[21] C. P. Liu, Phys. Rev. **C75**, 065501 (2007)

[22] D. M. Markoff, J. Res. Natl. Inst. Stand. Technol. **110**, 209 (2005)

[23] D. Tadic, Phys. Rev. **174**, 1694 (1968)

[24] G. S. Danilov, Phys. Lett. **B35**, 579 (1971)

[25] B. Desplanques, Nucl. Phys. **A 242**, 423 (1975)

[26] K. R. Lassey and B. H. J. McKellar, Nucl. Phys. **A260**, 413 (1976)

[27] S. Morioka, P. Grange, and Y. Avishai, Nucl. Phys. **A457**, 518 (1986)

[28] D. B. Kaplan, M. J. Savage, R. P. Springer, and M. B. Wise, Phys. Lett. **B449**, 1 (1999)

[29] B. Desplanques, Phys. Lett. **B512**, 305 (2001)

[30] M. J. Savage, Nucl. Phys. **A695**, 365 (2001)

[31] C. H. Hyun, T.-S. Park, and D.-P. Min, Phys. Lett. **B516**, 321 (2001)

[32] R. Schiavilla, J. Carlson, and M. W. Paris, Phys. Rev. **C67**, 032501 (2003)

[33] C. H. Hyun, S. J. Lee, J. Haidenbauer, and S. W. Hong, Eur. Phys. J. **A24**, 129 (2005)

[34] C. H. Hyun, S. Ando, and B. Desplanques, Eur. Phys. J. **A32**, 513 (2007)

[35] C. H. Hyun, S. Ando, and B. Desplanques, Phys. Lett. **B651**, 257 (2007)

[36] S.-i. Ando, C. H. Hyun, and J. W. Shin, Nucl. Phys. **A844**, 165 (2010)

[37] T. M. Partanen and J. A. Niskanen, Eur. Phys. J. **A47**, 53 (2011)

[38] V. G. J. Stoks, R. A. M. Klomp, C. P. F. Terheggen, and J. J. de Swart, Phys. Rev. **C49**, 2950 (1994)

[39] N. Kaiser, Phys. Rev. **C76**, 047001 (2007)

[40] B. Desplanques, C. H. Hyun, S. Ando, and C. P. Liu, Phys. Rev. **C77**, 064002 (2008)

[41] J. M. Blatt and V. F. Weisskopf, *Theoretical Nuclear Physics* (John Wiley and Sons Inc., New York, 1952)

[42] H. Rietschel, Nucl. Phys. **A 139**, 100 (1969)

[43] D. O. Riska and G. E. Brown, Phys. Lett. **B38**, 193 (1972)

[44] M. Simonius, Phys. Lett. **B73**, 13 (1978)

[45] A. E. Cox, S. A. R. Wynchank, and C. H. Collie, Nucl. Phys. **74**, 497 (1965)

[46] G. E. Brown and W. Weise, Phys. Rept. **22**, 279 (1975)